Long-term urban carbon dioxide observations reveal spatial and temporal dynamics related to urban characteristics and growth

Logan E. Mitchell[a,1], John C. Lin[a], David R. Bowling[b], Diane E. Pataki[b], Courtenay Strong[a], Andrew J. Schauer[c], Ryan Bares[a], Susan E. Bush[b], Britton B. Stephens[d], Daniel Mendoza[a], Derek Mallia[a], Lacey Holland[a,e], Kevin R. Gurney[f], and James R. Ehleringer[b]

[a]Department of Atmospheric Sciences, University of Utah, Salt Lake City, UT 84112; [b]Department of Biology, University of Utah, Salt Lake City, UT 84112; [c]Department of Earth and Space Sciences, University of Washington, Seattle, WA 98195; [d]National Center for Atmospheric Research, Boulder, CO 80307; [e]Department of Atmospheric Sciences, University of Hawaii at Manoa, Honolulu, HI 96822; and [f]School of Life Sciences, Arizona State University, Tempe, AZ 85287

Edited by Steven C. Wofsy, Harvard University, Cambridge, MA, and approved November 21, 2017 (received for review February 10, 2017)

Cities are concentrated areas of CO_2 emissions and have become the foci of policies for mitigation actions. However, atmospheric measurement networks suitable for evaluating urban emissions over time are scarce. Here we present a unique long-term (decadal) record of CO_2 mole fractions from five sites across Utah's metropolitan Salt Lake Valley. We examine "excess" CO_2 above background conditions resulting from local emissions and meteorological conditions. We ascribe CO_2 trends to changes in emissions, since we did not find long-term trends in atmospheric mixing proxies. Three contrasting CO_2 trends emerged across urban types: negative trends at a residential-industrial site, positive trends at a site surrounded by rapid suburban growth, and relatively constant CO_2 over time at multiple sites in the established, residential, and commercial urban core. Analysis of population within the atmospheric footprints of the different sites reveals approximately equal increases in population influencing the observed CO_2, implying a nonlinear relationship with CO_2 emissions: Population growth in rural areas that experienced suburban development was associated with increasing emissions while population growth in the developed urban core was associated with stable emissions. Four state-of-the-art global-scale emission inventories also have a nonlinear relationship with population density across the city; however, in contrast to our observations, they all have nearly constant emissions over time. Our results indicate that decadal scale changes in urban CO_2 emissions are detectable through monitoring networks and constitute a valuable approach to evaluate emission inventories and studies of urban carbon cycles.

urban | greenhouse gas | carbon dioxide | emissions | trends

Large amounts of carbon emissions from fossil fuel combustion are associated with urban areas, accounting for >70% of energy-related carbon dioxide (CO_2) emissions globally (1). Despite the increasing role that urban regions play in the global carbon budget, there are gaps in the current understanding of urban processes that influence carbon emissions (2, 3). Inventories of fossil fuel emissions are better constrained at national scales than at regional and local scales because energy consumption data are not publicly available except at aggregated spatial scales, and are reported with widely varying guidelines and procedures (2, 4–7). Atmospheric CO_2 observations can be used to quantify emissions, yet most long-term monitoring networks such as the National Oceanic and Atmospheric Administration's (NOAA) Global Greenhouse Gas Reference Network consist of "background sites" located far from urban areas to observe changes in the carbon cycle on continental-to-global spatial scales. Therefore, these networks are not suitable for evaluating emissions relevant to urban carbon dynamics.

The need to address urban carbon cycle knowledge gaps is driven by multiple factors (3, 8, 9). Stakeholders such as subnational cities and state governments have recently made commitments to reduce greenhouse gas emissions at the United Nations Conference of Parties in Paris (10, 11). Alliances such as the C40 Cities Climate Leadership Group and the Global Covenant of Mayors for Climate and Energy were formed to implement these policies as well as to share best practices for reducing urban emissions and adapting to climate risks. Reducing uncertainties associated with urban fossil fuel emissions will also improve our understanding of the global carbon budget, which is increasingly affected by errors in estimates of fossil fuel emissions in emerging economies (6). In addition, there is growing interest in reducing emissions of pollutants that are coemitted during fossil fuel combustion and which have large human health impacts (12–14). These stakeholder and scientific issues are dynamically changing as the prices of renewable energy are rapidly falling (15, 16), making the transition to renewable energy increasingly viable in an economic sense and the future of urban carbon emissions more difficult to predict.

Significance

Recent efforts to reduce greenhouse gas emissions have focused on cities due to intensive emissions, viable policy levers, and interested stakeholders. Atmospheric observations can be used to independently evaluate emissions, but suitable networks are sparse. We present a unique decadal record of atmospheric CO_2 from five sites with contrasting urban characteristics that show divergent trends in CO_2 emissions across a city. Comparison with population growth reveals a nonlinear relationship that may reflect how urban form affects CO_2 emissions. Four state-of-the-art global-scale emission inventories capture the nonlinear relationship with population density but not the divergent long-term trends across the city. This demonstrates that CO_2 monitoring networks can provide insight into urban carbon cycle processes and provide policy-relevant information to urban stakeholders.

Author contributions: L.E.M., D.R.B., D.E.P., C.S., and J.R.E. designed research; L.E.M., A.J.S., R.B., S.E.B., B.B.S., D. Mendoza, D. Mallia, L.H., and K.R.G. performed research; L.E.M. contributed new reagents/analytic tools; L.E.M., D. Mendoza, D. Mallia, and L.H. analyzed data; and L.E.M., J.C.L., D.R.B., D.E.P., C.S., K.R.G., and J.R.E. wrote the paper.

The authors declare no conflict of interest.

This article is a PNAS Direct Submission.

Data deposition: The CO_2 measurements, footprints, and other data are available at https://air.utah.edu/ and are archived with National Oceanic and Atmospheric Administration's (NOAA) National Centers for Environmental Information (NCEI) (https://doi.org/10.7289/V50R9MN2); the measurements are also archived with the Observation Package (ObsPack) Data Product (https://doi.org/10.15138/g3cw4q).

[1]To whom correspondence should be addressed. Email: logan.e.mitchell@gmail.com.

This article contains supporting information online at www.pnas.org/lookup/suppl/doi:10.1073/pnas.1702393115/-/DCSupplemental.

Published online March 5, 2018.

Urban CO_2 monitoring projects aim to address these challenges by providing crucial constraints on carbon cycling processes within cities. Long-term (>10 y) records exist only in a few cities such as Heidelberg, Germany (17, 18) and Pasadena, California (19, 20); however, these datasets were associated with a single long-term monitoring station in each city, limiting the ability to investigate spatial variability (3). Recently the Megacities Carbon Project (21) has built multisite networks in Los Angeles (including the long-term Pasadena site), and Paris (22) while other multisite networks have been established in other US cities: Portland, Oregon (23); Indianapolis (24, 25); Boston (26); Berkeley, California (27); and Washington, DC/Baltimore (28). The records from these cities, however, are not yet long enough to examine long-term (decadal) trends.

Here we present an urban dataset of continuous CO_2 mole fractions from a network of five sites within the Salt Lake Valley (SLV) and one background site in the Wasatch Mountains to the east of the SLV (Fig. 1) that have a range of urban settings (*SI Appendix*, Table S1). Prior research in the SLV examined valleywide diel/seasonal patterns of CO_2, attribution of CO_2 sources using isotopic signatures, the urban-to-rural CO_2 gradient, and emissions of the valley as a whole (12, 29–34). Here we present results on site-to-site differences on diel and seasonal timescales, long-term trends of CO_2 across an urban area, and the relationship between population density and fluxes.

Site Descriptions and Methodology

The SLV is located within Salt Lake County, Utah in the intermountain west of the continental United States and has a population of just over 1 million people (Salt Lake County 2010 census; https://www.census.gov/). It is bounded by the Wasatch and Oquirrh Mountains on the east and west sides of the valley, the Traverse Mountains to the south, and the Great Salt Lake to the northwest. The SLV CO_2 site locations, elevation, and inlet heights are listed in *SI Appendix*, Table S1 and the hourly averaged CO_2 mole fractions are shown in Fig. 1. Measurements were made every 5 min using nondispersive infrared gas analysis. Calibrations were conducted every 1 or 2 h depending on the site using working reference gas tanks with known CO_2 mole fractions traceable to the World Meteorological Organization CO_2 Mole Fraction Scales. *SI Appendix* and refs. 29 and 30 contain further details about the instrumentation and measurement procedures.

To evaluate the contribution of local processes to the measured CO_2 mole fraction, we subtracted CO_2 mole fractions representing background conditions from the hourly observations to obtain the "excess CO_2" of the urban atmosphere above background conditions. Background mole fractions (Fig. 1, black lines and *SI Appendix*) were obtained from a smoothed fit (35) applied to modeled CO_2 from Carbon Tracker (36) (Version CT2013B) from a region upstream of the SLV, as well as from the mountaintop CO_2 observation site at Hidden Peak (HDP) that represents free tropospheric mole fractions (37).

Spatiotemporal Patterns of Excess CO_2

Temporal patterns of CO_2 mole fractions have diel and seasonal components that reflect atmospheric mixing and emissions from both biological and anthropogenic sources. On diel timescales, the nighttime boundary layer is typically shallow, trapping emitted CO_2 near the ground resulting in elevated CO_2. After sunrise, daytime surface heating deepens the boundary layer, diluting surface emissions and entraining free tropospheric air with lower CO_2. These processes, along with photosynthetic uptake by plants, lead to reduced daytime surface CO_2 (33). On seasonal timescales, wintertime CO_2 is elevated due to increased natural gas combustion (29, 31) and persistent cold-air pools that trap emissions near the surface (12, 29, 33). Our goal here is to evaluate how these processes vary across the urban area and affect the diel and seasonal variations in CO_2. For this analysis we divided the year into a cold period (October–March) and a warm period (April–September) referred to as "winter" and "summer," respectively. Use of two periods rather than four conventional seasons was motivated by the gradual transition between warm-season low and cold-season high excess CO_2 (Fig. 2*A*).

The broad outlines of the excess CO_2 across the SLV, typically referred to as an "urban dome" (31, 38) are visible, with the Daybreak (DBK) and University of Utah (UOU) sites on the periphery of the urban dome having lower excess CO_2 while the Sugarhouse (SUG), Murray (MUR), and Rose Park (RPK) sites located within the urban dome have higher excess CO_2 (Fig. 2*A*).

Atmospheric mixing processes can be observed on diel and seasonal timescales (Fig. 2). On diel timescales, the location within the valley and topographic shading from the steep surrounding mountains determines the timing of solar heating and breakup of the nighttime boundary layer. The decline of excess CO_2 in the morning can be observed first at DBK on the southwestern margin of the SLV while the northeastern UOU site was the final site to respond. On seasonal timescales, the shorter winter days have fewer hours of low excess CO_2 in the afternoon than during summertime afternoons.

SUG had the largest winter–summer difference in monthly averaged excess CO_2 (Fig. 2*A*). This seasonal difference arises from nighttime CO_2 at SUG that is apparent compared with MUR and RPK (Fig. 2*B*), and may be due to the influence of household natural gas combustion, as this site is surrounded by residential housing. RPK had the highest summertime excess CO_2, especially apparent in the early evening. This site is located 2.9 km north of the largest electric utility generation facility in the SLV, within 10 km of five petroleum refineries, and 4 km east of the Salt Lake City International Airport. While most electricity consumed within the SLV is generated outside of the SLV and would therefore not contribute to CO_2 mole fractions

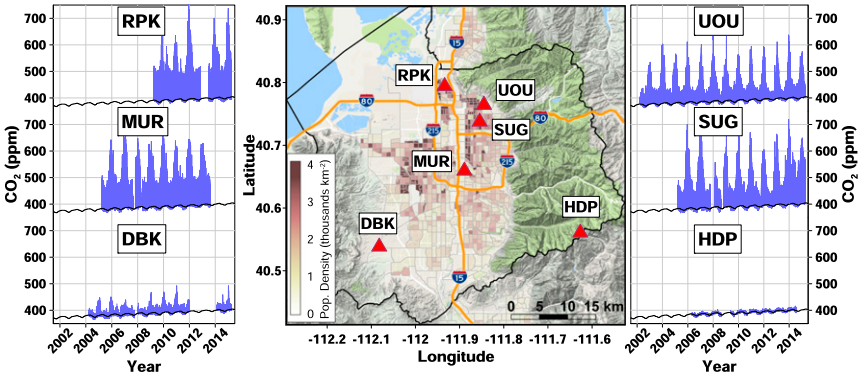

Fig. 1. SLV carbon dioxide measurement network. Time series show hourly averaged CO_2 mole fractions (blue) and the background CO_2 mole fractions derived from Carbon Tracker and the HDP site (black, *SI Appendix*). Population density is superimposed on the map and the black outline indicates Salt Lake County.

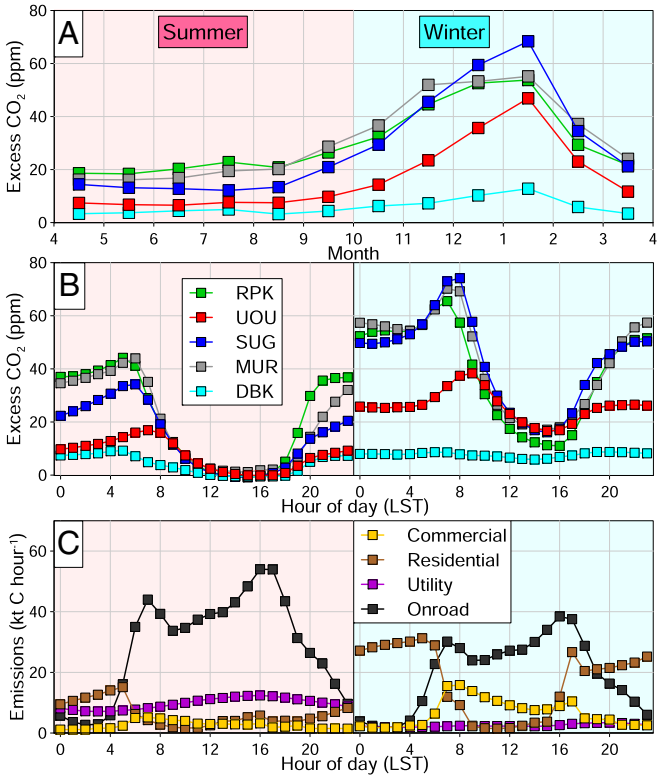

Fig. 2. Average monthly (*A*) and hourly (*B*) patterns of excess CO_2 from the SLV CO_2 sites as well as hourly patterns of CO_2 emissions for Salt Lake County derived from Hestia (*C*). In the hourly panels, the average during summer is on the left (pink shading) and the average during winter is on the right (blue shading).

within the valley, the facilities within the SLV are used when demand for electricity peaks. Hestia, a high-resolution, bottom-up CO_2 emissions model (39) that has been developed for the SLV (40) (Fig. 2, *Bottom*), indicates that emissions from electricity generation peak in the early evening in the summer (Fig. 2*C*) because of demand from air conditioning, which may explain the rapid increase in early evening excess CO_2 at RPK. During the winter this site had the lowest midafternoon excess CO_2 of all of the sites except for DBK, which was far from the urban center. Since there was minimal urban development between this site and the Great Salt Lake (~16 km northwest), we hypothesize that the low afternoon excess CO_2 was caused by onshore lake breezes (41) that carried air with CO_2 closer to background conditions from over the Great Salt Lake.

The DBK site exhibited negligible diel variability in the wintertime, contrary to the other sites. This was likely due to the site's location at the edge of the SLV urbanized area (42). At night when excess CO_2 mole fractions were typically elevated, the shallow boundary layer caused the site to be largely outside of the volume of air strongly influenced by local urban processes. As the onset of insolation triggered mixing of the air in the valley, this air mass expanded outward to include DBK, leading to higher mole fractions during the day. This pattern resulted in a relatively constant wintertime excess CO_2 diel profile (Fig. 2*B*).

Long-Term Trends in Excess CO_2

Long-term urban CO_2 records allow us to examine temporal urban carbon cycle changes across contrasting urban settings, and to evaluate hypotheses for these changes. Trends of excess CO_2 were calculated by first removing the seasonal cycle with a harmonic function fit and then calculating the least-squares linear regression and 2σ confidence intervals (35) (*SI Appendix*). We calculated trends from specific times to examine periods with consistent atmospheric mixing conditions [Fig. 3; Annual: all months; Winter: October–March; Summer: April–September; All hours: 00–23; Night: 00–05; Day: 12–17, Local Standard Time (LST)]. We used the average excess CO_2 for each day to represent statistically independent observations sufficiently devoid of autocorrelation (*SI Appendix*). Fig. 3*A* symbols show the mean excess CO_2 for that season and time of day calculated after gap filling the data to prevent biases from data gaps; however, the trends and error bounds were calculated before gap filling. Fig. 3*B* shows the slope and 2σ confidence intervals of the trends. The winter and summer time series are shown in *SI Appendix*, Fig. S11 as well as in a table listing the slope and 2σ confidence intervals (*SI Appendix*, Table S2).

The long-term excess CO_2 trends show divergent patterns across the SLV. In the northern SLV, RPK had a negative trend

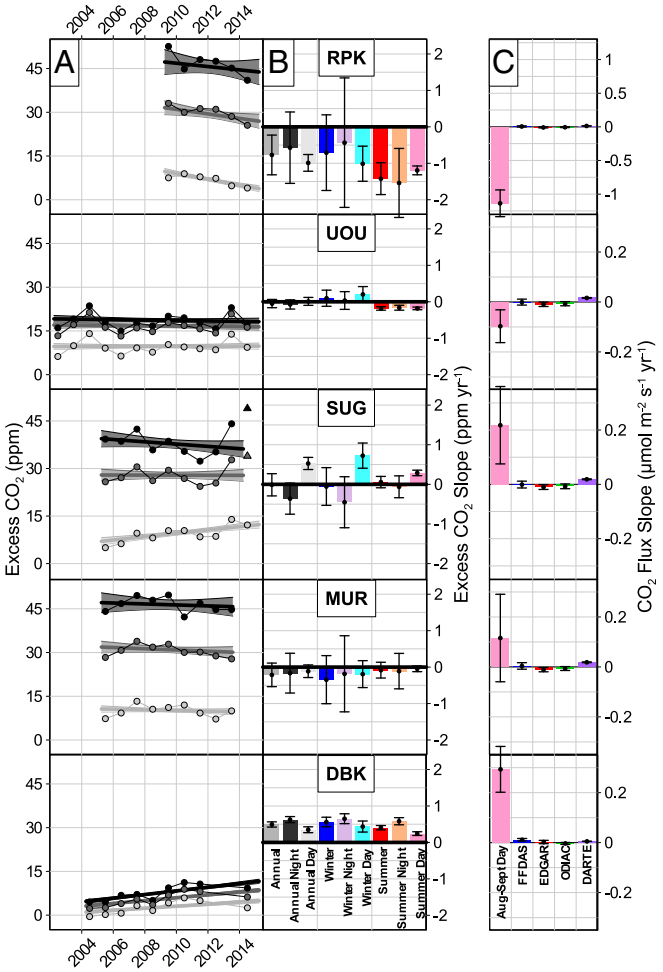

Fig. 3. Time series and trends in SLV excess CO_2 mole fractions calculated from daily averaged data, with shading indicating ±2σ confidence intervals (*A*). Time series for the cold-season winter period (October–March), and the warm-season summer period (April–September) are shown in *SI Appendix*. Each panel contains three trends: the central trend using data from all hours of the day, the upper trend using nighttime data, and the lower trend using daytime data (hourly delineations: All hours: 00–23; Night: 00–05; Day: 12–17, LST). Symbols represent the average mole fractions from each year–season–time of day combination. The final year (2014) of observations at SUG were elevated due to an anomalous contribution from an apparent local source and were not included in the trends for that site (triangle symbol, *SI Appendix*). *B* shows the slope for each season and time of day trend, with 2σ confidence intervals (numeric values are listed in *SI Appendix*, Table S2). *C* shows the slope of the F_{ff} trends derived from observations averaged in August and September as well as from four fossil fuel inventories with 2σ confidence intervals. Note that the RPK panel has a different scale. See *SI Appendix* for flux calculation details and sensitivity tests.

of −0.77 ± 0.54 ppm/y^{-1} ("Annual" in Fig. 3*B* and *SI Appendix*, Table S2). At the central and northeastern sites (UOU, SUG, MUR) the trends were small, with the slope of the Annual trends lacking statistical significance, but there were a few subtle seasonal and diel deviations from this overall pattern. Statistically significant negative trends were found during the summer at UOU, while positive daytime trends were found at SUG in both summer and winter. None of the other trends at these sites and MUR were statistically significant. Finally, in the southwestern SLV, DBK had a positive trend of 0.49 ± 0.07 ppm/y^{-1}.

Because urban CO_2 mole fractions are influenced by atmospheric mixing as well as anthropogenic emissions and biospheric exchange, we first examined atmospheric mixing proxies to evaluate potential explanations of temporal change. The planetary boundary layer (PBL) is the lowest region of the atmosphere where land–atmosphere exchange of CO_2 fluxes occurs, so changes in the depth of the PBL can impact observed CO_2. We examined the PBL height derived using the bulk Richardson method (43) from twice-daily radiosonde launches from the Salt Lake City International Airport and found that the percentage change in the PBL height is smaller than the relative magnitude of the 2σ confidence intervals of the excess CO_2 trends, meaning the excess CO_2 trends cannot be attributed to changes in the PBL height (*SI Appendix*). Since radiosonde observations were only available from the airport in the northern part of the SLV, we also compared surface temperatures at the airport and at a meteorological station near DBK to investigate whether surface warming in the southwest part of the valley could be causing additional turbulent mixing locally. We found that the magnitudes of temperature changes in the southwest part of the SLV were smaller than those at the airport, suggesting that the excess CO_2 trends at the DBK site also cannot be attributed to changes in atmospheric mixing. These observations are consistent with prior work that has found no long-term trend in other metrics for atmospheric mixing in this region (14). Since prior studies have found that biological fluxes had a minimal influence on overall emissions in the SLV (31, 33, 34), and research investigating future scenarios indicates that increasing urban vegetation cover would have a negligible effect on overall emissions (32), we explored factors that could explain temporal and spatial variations in drivers of anthropogenic CO_2 emissions as probable drivers of the excess CO_2 trends.

Prior work has indicated that anthropogenic CO_2 emissions are closely related to population distributions at broad spatial scales (e.g., state and national); however, the spatial pattern of emissions from different sectors becomes complex and less certain at finer spatial scales (e.g., urban) (6, 39, 44). For example, CO_2 emissions from electricity generation often occur at remote locations far from urban centers and are therefore uncorrelated with urban population patterns; furthermore, on-road emissions show nonlinearities with population density (45). Conversely, studies comparing nationally gridded emissions to population in urban areas have argued that emissions increase proportionally with urban size (46) or have superlinear scaling behavior (47), depending on how the urban boundaries are defined. A recent analysis of SLV emissions in 2011 using Hestia suggests that emissions from the residential sector exhibit slightly sublinear scaling with population at the census block group level (40).

To investigate the relationship between population and emissions, we have to consider the source region of emissions influencing the monitoring sites, i.e., the atmospheric footprint (48). We used the Stochastic Time-Inverted Lagrangian Transport model driven by meteorological fields from the Weather Research and Forecasting model (49) to generate mean midafternoon atmospheric footprints averaged over late summer (August and September) from 2007 and 2012 (*SI Appendix*). The time period of August to September was chosen to avoid the complex meteorology during the winter and to minimize the influence of biological fluxes, which are larger during the preceding months at the heart of the growing season. We compared the averaged footprints from 2007 and 2012 along with the inferred fluxes and found only small differences, so we assumed that the average footprint from the two years is a reasonable first-order approximation of summertime midafternoon transport in every year (*SI Appendix*). The averaged footprints were then used to calculate midafternoon fluxes of CO_2, from which we subtracted modeled biological fluxes to derive fossil fuel fluxes (F_{ff}). Slopes of the long-term F_{ff} trends are shown in Fig. 3*C*. The footprints were also used to examine the population changes (50) that the sites were sensitive to over time.

Overall, the footprint-weighted population increased by approximately equal amounts over the course of this study at each of the SLV sites (*SI Appendix*). Since the long-term trends in excess CO_2 and F_{ff} diverged between the sites, there must have been a nonlinear relationship between CO_2 emissions and population changes over time within the footprints of the stations. We further examined the population growth from rural (<1,000 people/mi^{-2}), suburban (1,000–5,000 people/mi^{-2}), and urban (>5,000 people/mi^{-2}) areas and found that the population growth in rural areas was twice as large within the DBK footprint compared with the other sites, while the growth in suburban and urbanized areas was more comparable between the sites (*SI Appendix*). The nonlinear relationship is illustrated by the comparison of summertime midafternoon F_{ff} versus the population density at each of the sites for every year (Fig. 4*A*). The relationship represented by the exponential curve fit is a function of the spatial pattern of emissions across the city (lower emissions in rural areas) as well as the temporal evolution of emissions that increased in low population density rural areas, but stabilized in suburban and urban areas with higher population densities. Since midafternoon summertime emissions come primarily from the on-road sector (Fig. 2), we hypothesize that the increasing fluxes at low population densities observed at DBK were driven by increased on-road emissions resulting from the conversion of undeveloped rural land into suburban developments. This is consistent with prior modeling looking at the entire United States that found on-road emissions were higher in suburban areas than in rural areas (44) and that emissions increased when rural areas were developed into suburban areas (45). Further, per-capita on-road emissions can decline at higher population densities, leading to stable CO_2 emissions even as total population increases (45), which is consistent with the stable CO_2 F_{ff} observed at the MUR, SUG, and UOU sites, even as population increased within the atmospheric footprints of these sites.

The RPK site deviates slightly from this overall relationship. This may be because the site was surrounded by multiple large industrial point sources, as noted earlier, with the largest being a natural-gas-fired electric utility power plant. Electricity generation and fuel consumption at this plant has declined by 40–50% since 2009 when RPK began observations, with considerable month-to-month variability (51). Electricity production declined in part because production has shifted outside of the SLV to newer, more efficient facilities. This decline in emissions represents a possible explanation for the negative excess CO_2 trend observed at RPK; however, the power plant is located between

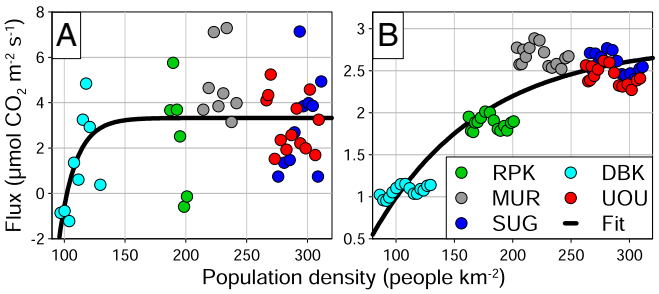

Fig. 4. Summer daytime fossil fuel CO_2 fluxes calculated from the observations (*A*) and from the FFDAS inventory (*B*) at each of the sites as a function of population density. Each point represents the summertime average flux from a specific year, with the flux calculation described in the text and *SI Appendix*. The black curve is an exponential function fit to the data.

the urban center and the site, making it difficult to disentangle these sources. More work is needed to evaluate this hypothesis.

Trends in Emission Models

The excess CO_2 trends can be compared with trends in nationally or globally gridded fossil fuel emission inventories across the SLV. Recently the spatial characteristics of gridded inventories have been compared (52) and here we build upon this by examining the decadal trends. Four inventories have sufficient temporal and spatial resolution to examine the SLV: EDGAR (Emission Database for Global Atmospheric Research) (53), FFDAS (Fossil Fuel Data Assimilation System) (54), ODIAC (Open source Data Inventory of Anthropogenic CO_2 emissions) (55), and DARTE (Database of Road Transportation Emissions) (45). EDGAR and ODIAC distribute national CO_2 emission estimates spatially with surrogates such as population, satellite-derived night lights, power plant locations, etc. FFDAS optimally solves an emissions model subject to the distributional constraint of nighttime lights, population, power plants, and a road basemap. DARTE is an on-road emissions inventory based on traffic count data and estimates of vehicle fleet composition; however, since it only includes the on-road sector, the magnitude of emissions is lower than the other inventories and we instead focus on the trends. The Hestia inventory is highly spatially resolved, but only a single year of emissions is currently available so a comparison over time is not yet possible.

In the SLV, the F_{ff} derived from the inventories are broadly consistent with the F_{ff} derived from the observations (*SI Appendix*); however, the simplified modeling framework we have implemented limits a comprehensive comparison of the magnitudes. A sensitivity test in *SI Appendix* explores this in greater depth. Since the global emission inventories spatially allocate national total emissions based on surrogate metrics they will, by definition, not entirely reflect local emissions (e.g., large industrial CO_2 emissions away from a given locale could be partly allocated inside the locale based on spatial surrogates such as night lights or population). Hence, we do not, a priori, expect close agreement between the trends in emissions and excess CO_2 trends. However, the purpose of these inventories is to examine subnational spatiotemporal emission patterns and our records provide the first opportunity for a comparison over time.

All four inventories indicate stable F_{ff} across the SLV over time, in contrast to the divergent trends we observe in the observationally derived F_{ff} (Fig. 3*C*). This is surprising, since we noted earlier that DARTE has a nonlinear relationship with population density in the United States. We find that within the SLV, the nonlinear relationship is present in all four inventories, but it is driven entirely by a fixed spatial pattern of emissions (as demonstrated by FFDAS in Fig. 4*B*; the other inventories are shown in *SI Appendix*), as opposed to the observations where the nonlinear relationship is driven by both spatial and temporal changes in emissions (Fig. 4*A*). There are several possible explanations for the different spatiotemporal changes across the SLV in the emission inventories. A close examination of the F_{ff} time series shows that the inventories that rely on downscaled national emissions (EDGAR, ODIAC) are highly correlated with US total emissions, indicating that their temporal variability is driven primarily by national emissions and not by temporal changes in their spatial allocation proxies (*SI Appendix*). This is compounded by the inventories not always reflecting the emissions of a given locale because of the relationship between industrial emitters and consumers. Also, inventories that use a constant road basemap (DARTE, FFDAS) may not have captured emissions associated with the growth in the road network and associated on-road emissions when rural areas were developed into suburban developments. These comparisons demonstrate some of the challenges facing urban applications of current global emission inventories that use spatial proxies to distribute emissions as well as the potential for future improvements, such as using long-term multisite urban records to calibrate spatial allocation proxies to better reflect local trends in emissions. Future work should also investigate high-resolution emission models (e.g., Hestia) that are optimized for urban emissions and incorporate local emissions information that can enable a more detailed comparison with multiple atmospheric monitoring locations over time.

Conclusions

This study shows that long-term, spatially distributed urban CO_2 monitoring networks yield insights into the carbon budgets of urban areas that contain an increasing fraction of the world's population. These urban atmospheric CO_2 observations integrate atmospheric processes, biospheric exchange, and temporal changes in emissions related to urbanization processes such as changing transportation patterns and suburban growth. Changes in F_{ff} were likely the primary driver of long-term trends in excess CO_2 in the SLV as there were negligible changes in atmospheric mixing and prior studies concluded that biospheric processes had minimal effects on overall emissions. We draw several conclusions from our analysis of the long-term trends. First, divergent CO_2 emission trends were detected despite similar levels of population growth and thus, changes in urban fossil fuel CO_2 emissions likely did not scale linearly with population changes. Rapidly increasing daytime emission rates during the summer occurred in areas with initially low population density that underwent conversion of rural land to suburban developments while emissions were stable in the urban core despite population increases, consistent with prior modeling efforts examining changes in on-road emissions over space and time (44, 45). While excess CO_2 trends in other urban centers with established monitoring programs are also "likely stable" (3), this does not account for changing emissions in rapidly expanding suburban areas, with important implications for policy makers who want to take greenhouse gas emissions into account in urban growth planning. These spatiotemporal patterns and contrasting trends may be representative of urban transitions in many US cities that have stabilizing emissions in their urban cores, and expanding suburban growth. Second, trends in the northern, industrial part of the SLV declined coincident with a reduction in power production by a nearby electric utility power plant, representing a possible explanation for the decline and highlighting the importance of large urban point sources. Third, state-of-the-art gridded emission inventories with sufficient spatial resolution and temporal coverage indicate relatively stable emissions in the SLV, while our observations point to divergent trends in F_{ff}. The divergent trends contribute to a nonlinear relationship between population density and CO_2 emissions. This nonlinear relationship also is evident in the emission inventories because of the spatial pattern of emissions, but it is muted by the lack of temporal trends. These comparisons can provide key metrics to evaluate emission inventories over time. Incorporation of data from local emissions sources, to the extent possible, could provide improved agreement with the observations.

Our observations support the conclusion that multiple monitoring stations are needed to track urban CO_2 emissions (56). Furthermore, our observations suggest that urban CO_2 networks that do not also include sites sensitive to expanding urban and suburban areas could miss important changes in carbon fluxes. Capturing and understanding patterns in suburban areas is important as they tend to have a higher household carbon footprint than urban centers (44). Therefore, anticipating urban and suburban growth patterns has a role for monitoring network design.

Finally, our data show that changes in CO_2 emissions are detectable in urban monitoring networks on a decadal scale, especially when long-term emission trends and observations are linked through atmospheric inversion modeling. Our initial efforts should be expanded with temporally explicit atmospheric transport modeling to resolve the spatiotemporal evolution of carbon emissions in the SLV that can be compared quantitatively with detailed emissions inventories or highly resolved estimates of CO_2 emissions such as Hestia (39). As other cities establish long-term, multisite CO_2 observation networks of sufficient

duration, intercity and intracity comparisons will become possible, leading to further insights into how dynamic urbanization processes impact the carbon cycle and the development of tools for stakeholders to evaluate emission mitigation efforts.

ACKNOWLEDGMENTS. We thank Hillcrest Junior High School and the Salt Lake Center for Science Education for hosting CO_2 monitoring sites as well as Dean Cardinale and Snowbird Ski Area staff for assistance with the HDP site. Thanks also to MesoWest for providing historic meteorological data, NOAA Earth System Research Laboratory (ESRL) for providing CO_2 observations from Wendover, Utah, and three anonymous reviewers who provided constructive feedback that improved the manuscript. CarbonTracker CT2013B results were provided by NOAA ESRL from https://www.esrl.noaa.gov/gmd/ccgg/carbontracker/. The National Center for Atmospheric Research is sponsored by NSF. This work was supported by Department of Energy (DOE) Grants DE-SC-001-0624, DE-FG02-04ER63904, DE-SC0005236, and DE-SC0010625; NSF Grants EF-1137336, EF-01241286, and EF-01240142; and NOAA Grant NA14OAR4310178. The HDP measurements were supported by NSF (EAR-0321918), NOAA (NA09OAR4310064), and DOE (DE-SC0010624 and DE-SC0010625); the data can be downloaded from https://www.eol.ucar.edu/homes/stephens/RACCOON/.

1. International Energy Agency (2008) *World Energy Outlook 2008* (International Energy Agency, Paris).
2. Pataki DE, et al. (2006) Urban ecosystems and the North American carbon cycle. *Glob Change Biol* 12:2092–2102.
3. Hutyra LR, et al. (2014) Urbanization and the carbon cycle: Current capabilities and research outlook from the natural sciences perspective. *Earths Future* 2:473–495.
4. Ackerman KV, Sundquist ET (2008) Comparison of two U.S. power-plant carbon dioxide emissions data sets. *Environ Sci Technol* 42:5688–5693.
5. NRC (2010) *Verifying Greenhouse Gas Emissions: Methods to Support International Climate Agreements* (National Academies Press, Washington, DC).
6. Andres RJ, et al. (2012) A synthesis of carbon dioxide emissions from fossil-fuel combustion. *Biogeosciences* 9:1845–1871.
7. Kennedy C, Demoullin S, Mohareb E (2012) Cities reducing their greenhouse gas emissions. *Energy Policy* 49:774–777.
8. Rosenzweig C, Solecki W, Hammer SA, Mehrotra S (2010) Cities lead the way in climate-change action. *Nature* 467:909–911.
9. Gurney KR, et al. (2015) Climate change: Track urban emissions on a human scale. *Nature* 525:179–181.
10. OECD/IEA (2009) *Cities, Towns & Renewable Energy: Yes in My Front Yard* (OECD/IEA, Paris).
11. Global Climate Action–NAZCA. Available at http://climateaction.unfccc.int/. Accessed May 28, 2017.
12. Pataki DE, et al. (2005) Can carbon dioxide be used as a tracer of urban atmospheric transport? *J Geophys Res Atmos* 110:D15102.
13. West JJ, et al. (2013) Co-benefits of mitigating global greenhouse gas emissions for future air quality and human health. *Nat Clim Chang* 3:885–889.
14. Whiteman CD, Hoch SW, Horel JD, Charland A (2014) Relationship between particulate air pollution and meteorological variables in Utah's Salt Lake Valley. *Atmos Environ* 94:742–753.
15. MacDonald AE, et al. (2016) Future cost-competitive electricity systems and their impact on US CO2 emissions. *Nat Clim Chang* 6:526–531.
16. Haegel NM, et al. (2017) Terawatt-scale photovoltaics: Trajectories and challenges. *Science* 356:141–143.
17. Vogel FR, et al. (2013) Can we evaluate a fine-grained emission model using high-resolution atmospheric transport modelling and regional fossil fuel CO_2 observations? *Tellus B Chem Phys Meterol* 65:18681.
18. Levin I, Hammer S, Eichelmann E, Vogel FR (2011) Verification of greenhouse gas emission reductions: The prospect of atmospheric monitoring in polluted areas. *Philos Trans A Math Phys Eng Sci* 369:1906–1924.
19. Newman S, Xu X, Affek HP, Stolper E, Epstein S (2008) Changes in mixing ratio and isotopic composition of CO2 in urban air from the Los Angeles basin, California, between 1972 and 2003. *J Geophys Res Atmos* 113:D23304.
20. Newman S, et al. (2016) Toward consistency between trends in bottom-up CO2 emissions and top-down atmospheric measurements in the Los Angeles megacity. *Atmos Chem Phys* 16:3843–3863.
21. Duren RM, Miller CE (2012) Measuring the carbon emissions of megacities. *Nat Clim Chang* 2:560–562.
22. Bréon FM, et al. (2015) An attempt at estimating Paris area CO2 emissions from atmospheric concentration measurements. *Atmos Chem Phys* 15:1707–1724.
23. Rice A, Bostrom G (2011) Measurements of carbon dioxide in an Oregon metropolitan region. *Atmos Environ* 45:1138–1144.
24. Turnbull JC, et al. (2015) Toward quantification and source sector identification of fossil fuel CO2 emissions from an urban area: Results from the INFLUX experiment. *J Geophys Res Atmos* 120:292–312.
25. Lauvaux T, et al. (2016) High resolution atmospheric inversion of urban CO2 emissions during the dormant season of the Indianapolis Flux Experiment (INFLUX). *J Geophys Res Atmos* 121:5213–5236.
26. Briber BM, Hutyra LR, Dunn AL, Raciti SM, Munger JW (2013) Variations in atmospheric CO2 mixing ratios across a Boston, MA urban to rural gradient. *Land (Basel)* 2:304–327.
27. Shusterman AA, et al. (2016) The BErkeley atmospheric CO2 observation network: Initial evaluation. *Atmos Chem Phys* 16:13449–13463.
28. Lopez-Coto I, Ghosh S, Prasad K, Whetstone J (2017) Tower-based greenhouse gas measurement network design—The National Institute of Standards and Technology North East Corridor Testbed. *Adv Atmos Sci* 34:1095–1105.
29. Pataki DE, Bowling DR, Ehleringer JR (2003) Seasonal cycle of carbon dioxide and its isotopic composition in an urban atmosphere: Anthropogenic and biogenic effects. *J Geophys Res Atmos* 108:4735.
30. Pataki DE, Bowling DR, Ehleringer JR, Zobitz JM (2006) High resolution atmospheric monitoring of urban carbon dioxide sources. *Geophys Res Lett* 33:L03813.
31. Pataki DE, Xu T, Luo YQ, Ehleringer JR (2007) Inferring biogenic and anthropogenic carbon dioxide sources across an urban to rural gradient. *Oecologia* 152:307–322.
32. Pataki DE, et al. (2009) An integrated approach to improving fossil fuel emissions scenarios with urban ecosystem studies. *Ecol Complex* 6:1–14.
33. Strong C, Stwertka C, Bowling DR, Stephens BB, Ehleringer JR (2011) Urban carbon dioxide cycles within the Salt Lake Valley: A multiple-box model validated by observations. *J Geophys Res Atmos* 116:D15307.
34. McKain K, et al. (2012) Assessment of ground-based atmospheric observations for verification of greenhouse gas emissions from an urban region. *Proc Natl Acad Sci USA* 109:8423–8428.
35. Thoning KW, Tans PP, Komhyr WD (1989) Atmospheric carbon dioxide at Mauna Loa Observatory: 2. Analysis of the NOAA GMCC data, 1974–1985. *J Geophys Res Atmos* 94:8549–8565.
36. Peters W, et al. (2007) An atmospheric perspective on North American carbon dioxide exchange: CarbonTracker. *Proc Natl Acad Sci USA* 104:18925–18930.
37. Stephens BB, Miles NL, Richardson SJ, Watt AS, Davis KJ (2011) Atmospheric CO2 monitoring with single-cell NDIR-based analyzers. *Atmos Meas Tech* 4:2737–2748.
38. Idso CD, Idso SB, Balling RC, Jr (2001) An intensive two-week study of an urban CO2 dome in Phoenix, Arizona, USA. *Atmos Environ* 35:995–1000.
39. Gurney KR, et al. (2012) Quantification of fossil fuel CO2 emissions on the building/street scale for a large U.S. city. *Environ Sci Technol* 46:12194–12202.
40. Patarasuk R, et al. (2016) Urban high-resolution fossil fuel CO2 emissions quantification and exploration of emission drivers for potential policy applications. *Urban Ecosyst* 19:1013–1039.
41. Crosman ET, Horel JD (2016) Winter lake breezes near the Great Salt Lake. *Boundary-Layer Meteorol* 159:439–464.
42. Stwertka CH (2012) Carbon dioxide variability within the urban Salt Lake Valley: An observational and modeling study. MS thesis (University of Utah, Salt Lake City). Available at https://search.proquest.com/docview/1451451379. Accessed May 3, 2016.
43. Seidel DJ, Ao CO, Li K (2010) Estimating climatological planetary boundary layer heights from radiosonde observations: Comparison of methods and uncertainty analysis. *J Geophys Res Atmos* 115:D16113.
44. Jones C, Kammen DM (2013) Spatial distribution of U.S. household carbon footprints reveals suburbanization undermines greenhouse gas benefits of urban population density. *Environ Sci Technol* 48:895–902.
45. Gately CK, Hutyra LR, Sue Wing I (2015) Cities, traffic, and CO2: A multidecadal assessment of trends, drivers, and scaling relationships. *Proc Natl Acad Sci USA* 112:4999–5004.
46. Fragkias M, Lobo J, Strumsky D, Seto KC (2013) Does size matter? Scaling of CO2 emissions and US urban areas. *PLoS One* 8:e64727.
47. Oliveira EA, Andrade JS, Jr, Makse HA (2014) Large cities are less green. *Sci Rep* 4:4235.
48. Lin JC, et al. (2003) A near-field tool for simulating the upstream influence of atmospheric observations: The Stochastic Time-Inverted Lagrangian Transport (STILT) model. *J Geophys Res* 108:ACH 2-1–ACH 2-17.
49. Skamarock WC, Klemp JB (2008) A time-split nonhydrostatic atmospheric model for weather research and forecasting applications. *J Comput Phys* 227:3465–3485.
50. US Census Bureau (2015) Population estimates–City and town totals: Vintage 2014. Available at https://www.census.gov/programs-surveys/popest/data/tables.html. Accessed July 8, 2015.
51. EIA (2015) Electricity data browser–Gadsby. Available at www.eia.gov/electricity/data/browser/#/plant/3648. Accessed October 18, 2015.
52. Hutchins MG, Colby JD, Marland G, Marland E (2016) A comparison of five high-resolution spatially-explicit, fossil-fuel, carbon dioxide emission inventories for the United States. *Mitig Adapt Strateg Glob Change* 22:947–972.
53. Olivier JGJ, et al. (2005) Recent trends in global greenhouse gas emissions: Regional trends 1970–2000 and spatial distributionof key sources in 2000. *Environ Sci* 2:81–99.
54. Asefi-Najafabady S, et al. (2014) A multiyear, global gridded fossil fuel CO2 emission data product: Evaluation and analysis of results. *J Geophys Res Atmos* 119:10213–10231.
55. Oda T, Maksyutov S (2011) A very high-resolution (1 km×1 km) global fossil fuel CO2 emission inventory derived using a point source database and satellite observations of nighttime lights. *Atmos Chem Phys* 11:543–556.
56. Kort EA, Angevine WM, Duren R, Miller CE (2013) Surface observations for monitoring urban fossil fuel CO_2 emissions: Minimum site location requirements for the Los Angeles megacity. *J Geophys Res Atmos* 118:1577–1584.